Nuclear Instruments and Methods in Physics Research A 613 (2010) 207–217

Contents lists available at ScienceDirect

Nuclear Instruments and Methods in Physics Research A

journal homepage: www.elsevier.com/locate/nima

The internal alignment and position resolution of the AMS-02 silicon tracker determined with cosmic-ray muons

B. Alpat [a], G. Ambrosi [a], Ph. Azzarello [a], R. Battiston [b], B. Bertucci [b], M. Bourquin [c], W.J. Burger [a], F. Cadoux [c], C.F. da Silva Costa [c], V. Choutko [d], M. Duranti [b], E. Fiandrini [b], D. Haas [c], S. Haino [a,*], M. Ionica [a], R. Ionica [e], C. Lechanoine-Leluc [c], M. Menichelli [a], S. Natale [c,1], A. Oliva [b], M. Paniccia [c], E. Perrin [c], M. Pohl [c], D. Rapin [c], N. Tomassetti [b], P. Zuccon [a], C. Zurbach [f]

[a] INFN Sezione di Perugia, I-06100 Perugia, Italy
[b] INFN Sezione di Perugia and Università degli Studi di Perugia, I-06100 Perugia, Italy
[c] Université de Genève, CH-1211, Geneve 4, Switzerland
[d] Massachusetts Institute of Technology, Cambridge, MA 02139, USA
[e] University Politechnica (UPB), R-76900 Bucharest, Romania
[f] Laboratoire de Physique Thèorique et Astroparticules, IN2P3/CNRS, Université de Montpellier II, F-34095 Montpellier, France

ARTICLE INFO

Article history:
Received 15 August 2009
Received in revised form
9 November 2009
Accepted 24 November 2009
Available online 16 December 2009

Keywords:
Charged particle spectrometers
Tracking and position sensitive detectors
Cosmic-ray detectors

ABSTRACT

The Alpha Magnetic Spectrometer is a large acceptance cosmic-ray detector (0.5 m^2sr) designed to operate at an altitude of 400 km on the International Space Station. The AMS-02 silicon tracker contains 2264 silicon microstrip sensors (total active area 6.75 m^2). The internal alignment parameters of the assembled tracker have been determined on the ground with cosmic-ray muons. The alignment procedure is described and results for the alignment precision and position resolution are reported.

1. Introduction

The Alpha Magnetic Spectrometer (AMS) is a large acceptance cosmic-ray detector which will be installed as an independent module on the International Space Station (ISS). The instrument will provide a precise measurement of the cosmic-ray energy spectra and extensive antimatter search up to several TeV for particle charges up to $Z=26$. A preliminary version of the detector AMS-01, with a permanent magnet and six-layer silicon tracker, was flown on NASA space shuttle *Discovery* in June 1998 [1]. The second generation detector AMS-02 (Fig. 1) contains a superconducting magnet (0.8 T) and an eight-layer silicon tracker. The AMS-02 tracker provides multiple measurements of the specific energy loss of the charged particle, which are combined with the velocity measurements provided by the time-of-flight scintillators and the ring-imaging Cherenkov detector to determine the magnitude of the particle charge. The latter and the position measurements of the tracker in the 0.8 T field are used to determine the rigidity and the sign of the charge.

The tracker is composed of 2264 double-sided silicon microstrip sensors positioned with high precision in 192 electrically and mechanically independent modules called ladders. A limited number (4–11) of ladders have been exposed to several particle beams to evaluate their performance. A detailed description of the ladders, as well as results for the position resolution and detection efficiency of the AMS-02 ladders for relativistic protons and helium nuclei are found in Ref. [2]. Results for the charge determination for relativistic nuclei from $Z=1$ to 26 have been reported in Ref. [3].

In this paper we report the performance of the fully assembled tracker in terms of its position resolution evaluated with cosmic muon tracks registered without the magnetic field during the pre-integration phase of the AMS-02 spectrometer, which lasted from September 2007 to June 2008. A position resolution of 10 (30) μm along the bending (non-bending) direction is expected for a single ladder. Full exploitation of the ladder spatial resolution in the track reconstruction requires the accurate knowledge of ladder positions within the assembled tracker. An iterative procedure has been developed to perform alignment of the tracker, i.e. to evaluate the actual ladder positions in the tracker with respect to the nominal design.

The basic characteristics of the AMS-02 silicon tracker (Section 2) and its operation during the cosmic-ray data taking (Section 3)

* Corresponding author.
E-mail address: Sadakazu.HAINO@pg.infn.it (S. Haino).
[1] Now at Physikalisches Institut RWTH, D-52056 Aachen, Germany.

0168-9002/$ - see front matter © 2009 Elsevier B.V. All rights reserved.
doi:10.1016/j.nima.2009.11.065

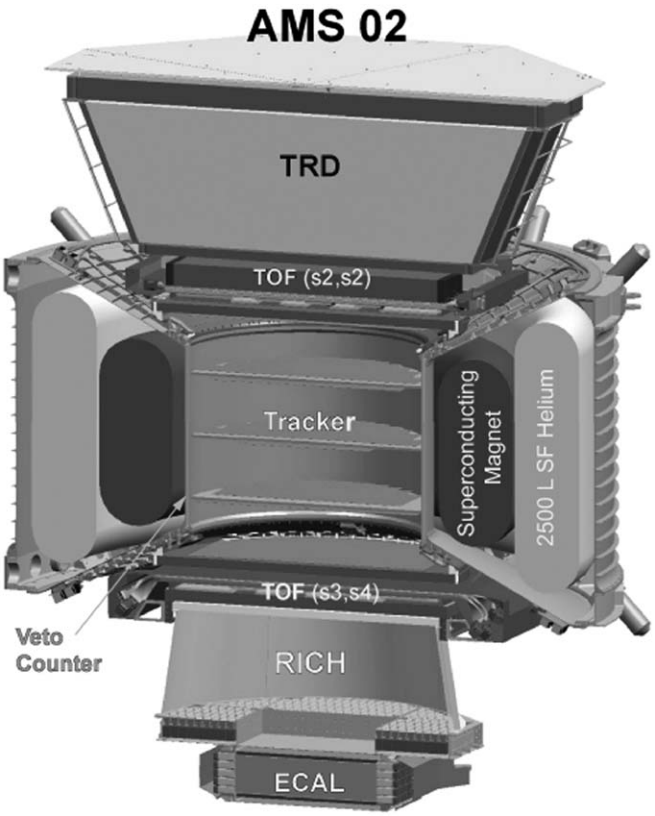

Fig. 1. Schematic view of the AMS-02 spectrometer.

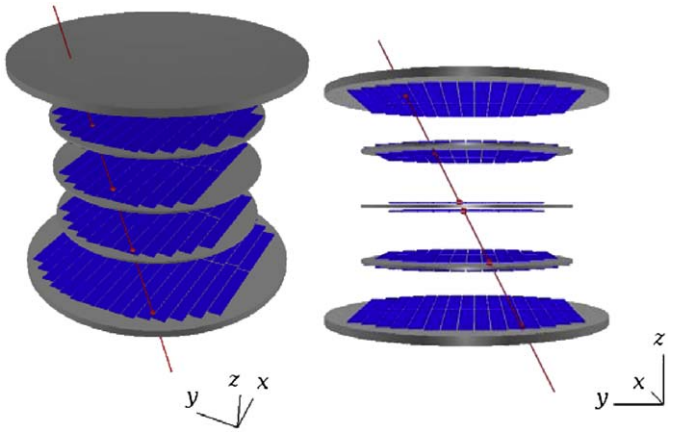

Fig. 2. Three-dimensional views of a reconstructed cosmic-ray muon track in the AMS-02 tracker from the May 2008 data sample.

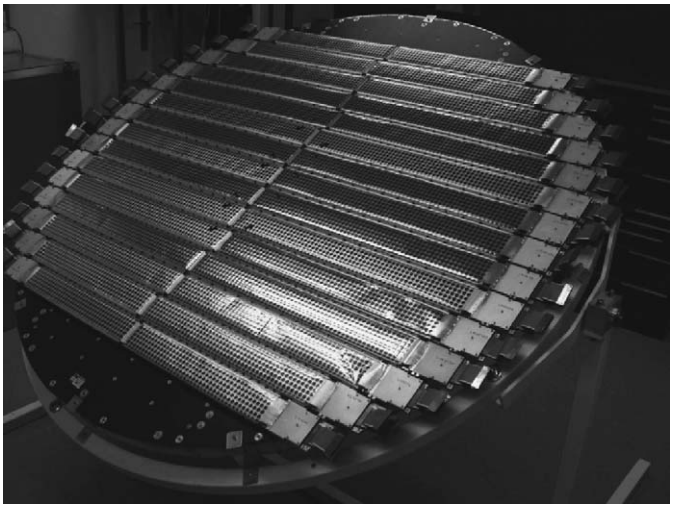

Fig. 3. Silicon ladders mounted on an external tracker plane.

are first introduced. The procedure of the hit and track reconstruction and the alignment calibration are then described (Section 4). As results of this work, the stability of the alignment parameters derived from different data samples and the position resolution estimated after the alignment are presented. The paper concludes with a discussion on the expected rigidity resolution of the superconducting magnet spectrometer (Section 5).

2. The silicon tracker

The AMS-02 tracker contains 2264, $41.360 \times 72.045 \times 0.300\,\mathrm{mm}^3$, double-sided silicon microstrip sensors[2] with a total active area $6.75\,\mathrm{m}^2$. A variable number of sensors (7–15) is arranged in independent ladder units. The sensor alignment precision is given by the dowel pin position precision ($\sim 2\,\mu\mathrm{m}$) and the mechanical tolerance of the wafer cut ($< 5\,\mu\mathrm{m}$) [4]. The 192 ladders are arranged in eight layers on five support planes to fill the circular plane geometry as schematically shown in Fig. 2 with a reconstructed cosmic-ray muon track. The two outermost silicon layers are separated by a distance of 1.06 m and located on the first and last support planes at both ends of the spectrometer, just outside the magnet. One of the two external planes is shown in Fig. 3. Double silicon layers are disposed on both sides of the three support planes located inside the magnetic volume as shown in Fig. 4. All the support planes are made of an aluminum honeycomb structure enclosed within thin carbon fiber skins: a larger diameter ($d = 1.4\,\mathrm{m}$) and higher density ($\rho = 0.032\,\mathrm{g/cm}^2$) characterize the two external planes with respect to the internal ones ($d = 1\,\mathrm{m}, \rho = 0.016\,\mathrm{g/cm}^2$). The total thickness of one internal plane including two silicon layers and one support plane is about 1% of radiation length (X/X_0).

On opposite sides of the silicon sensor, p^+ (junction) and n^+ (ohmic) strips are implanted along orthogonal directions with implantation (readout) pitches of 27.5(110) μm and 104[3] (208) μm, respectively. The p-side strips provide the measurement of the bending coordinate in the spectrometer: running along the ladder length, the strips from different sensors are daisy chained up to the ladder end where they are connected to an hybrid, which provide bias voltages and front-end readout chips. The n-side strips, providing the measurement of the non-bending coordinate, are also routed to the ladder end by means of a kapton cable which distributes signals of alternating sensors to the same readout channel. The 640 (384) readout strips from the p (n) sides of each ladder are ac-coupled to a 64 channel low-noise, high dynamic range readout chip the VA64_hdr9a[4] via 700 pF capacitor. The analog signals of each hybrid pair, for p and n side, are transferred to a Tracker Data Reduction (TDR) module, which contains 12-bit ADCs, Field Programmable Gate Arrays (FPGA) and Digital Signal Processors (DSP) for data reduction.

[2] Fabricated by Colibrys SA, Maladière 83, 2000 Neuchâtel, Switzerland and FBK-irst, Via Sommarive 18, 38050 Provo, Italy.

[3] 52 μm including p^+ blocking strips.

[4] The VA series of multi-channel ASICs, Gamma Medica - Ideas AS, Martin Linges vei 25, Snaroy, POB 1, N-1330 Fornebu, Norway.

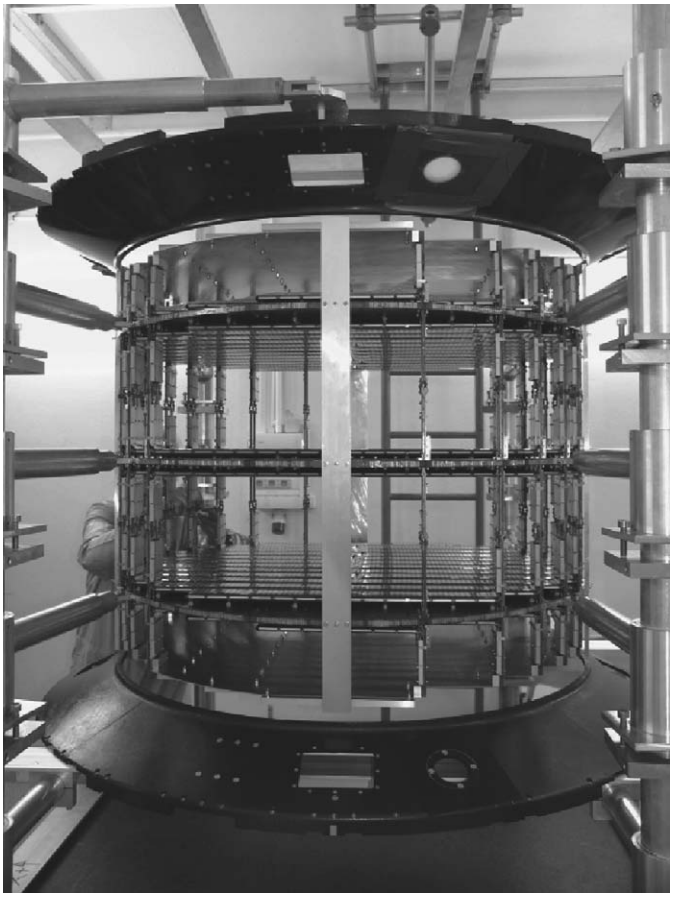

Fig. 4. The three internal planes in the tracker assembly jig at the Université de Genève. The conical sections, which support the two external ladder planes at the entrance and exit of the magnet, are visible at the top and bottom of the cylindrical volume.

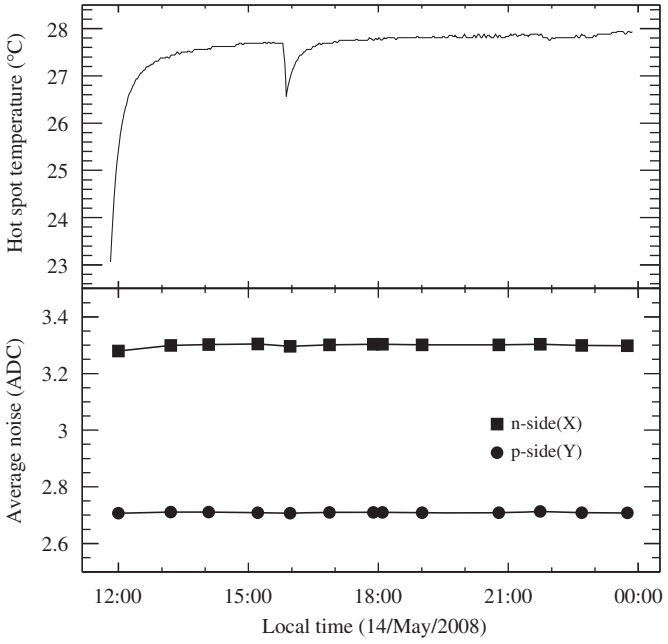

Fig. 5. Temperature profile on a hot spot close to the front-end electronics during the day of May/14/2008 (top), and average channel noise of all the ladders in p-side shown with filled circles and n-side shown with filled squares (bottom). The channel noise is defined as a root-mean-square of the pedestal ADC count taken in the calibration run.

The ADC values of the readout strips include a pedestal, a common noise, a strip noise and an eventual signal. The mean and root mean square (RMS) of the pedestal are determined in a calibration run, usually at the beginning or the end of a scientific run. The common noise is computed at the level of the VAs for each event. A valid signal is defined by a threshold applied to the strip signal-to-noise ratio, where signal refers to the ADC value after the pedestal and common noise subtraction, and noise refers to the RMS value obtained in the calibration run. All the above process is done online by the DSP on the TDR boards. Thus the recorded data contain only strips with potential signal called raw clusters.

3. Cosmic-ray data

In the pre-integration phase of the AMS spectrometer from September 2007 to June 2008, all the detector subsystems were integrated into the prototype vacuum case of the magnet. Tracker data were taken without magnetic field with a trigger generated by Time-Of-Flight (TOF) scintillator planes for six months in total, including a debugging phase. In the last two months (May and June 2008) the full tracker was connected with the Data Acquisition (DAQ) system and a simplified version of the thermal control system. Fig. 5 shows a temperature profile of a hot spot close to the front-end electronics during the day of May/14/2008 and the average channel noise of all the readout channels, which is defined as the RMS of the pedestal ADC count taken in calibration runs. Despite the large increase of the temperature after turning the system on, the noise level was kept stable thanks to the weak thermal coupling between the front-end electronics and the silicon sensors. The low and stable noise level enabled us to achieve an average cluster signal-to-noise ratio of 7.2 on the p-side and 6.6 on the n-side for vertical muon incidence, where the cluster signal-to-noise ratio is defined as an ADC sum of the signal strips divided by the average channel noise.

During the full tracker test 90 million events were taken without magnetic field. Vertical position of the spectrometer, with the tracker planes orthogonal to gravity, was the nominal run condition. Rotation of the whole spectrometer in the vertical plane up to 90° was performed during the last tens runs dedicated to the study of the tracker mechanical stability. The data were divided into 13 data sets, each with about one million reconstructed tracks, as listed in Table 1. The trigger of the data acquisition system was generated with a coincidence of signals from any two TOF layers out of four. Because of this loose trigger condition, about 10% of the events had tracks fully contained in the tracker. The track to trigger ratio is lower for larger rotation angles as the muon flux decreases rapidly for larger zenith angle. The reconstructed track rates for 0° (nominal), 30°, 60°, and 90° were 37 Hz, 29 Hz, 14 Hz, and 5.6 Hz, respectively, and agreed well with estimations based on a muon flux calculated as a function of zenith angle [6].

4. Data processing

In this section, the procedures applied to pass from raw data to reconstructed tracks are briefly summarized. Then the alignment procedure is presented and discussed. Details about ladder efficiency and charge identification capability can be found in Refs. [2,3].

Table 1
Summary of data sets used in this analysis.

ID	Date	Number of triggers ($\times 10^6$)	Number of tracks ($\times 10^5$)	Position
M001	7/May	8.54	9.06	
M002	8, 9/May	10.42	11.87	
M003	13/May	12.12	12.42	0° rotation
M004	14/May	13.79	12.50	
M005	15/May	8.81	9.62	
M000	8–15/May	53.68	55.47	Sum of M001–M005
J000	10/June	0.56	0.58	0° rotation
J30p	10/June	3.86	3.44	+30° rotation
J90p	10, 11/June	7.04	1.92	+90° rotation
J60p	11, 12/June	3.42	1.85	+60° rotation
J30n	12/June	1.62	1.45	−30° rotation
J60n	12/June	2.10	1.13	−60° rotation
J90n	12, 13/June	5.46	1.49	−90° rotation
J001	13, 14/June	11.83	12.14	0° rotation

4.1. Three dimensional hit reconstruction

The tracker raw data are the outputs of the TDR data compression, which are presented on a per ladder basis and are made of a list of raw clusters in terms of readout channels. Given the limitations on the TDR power consumption and the processing time, the compression algorithm is minimized and cannot handle special cases. The first step in the hit reconstruction is then to expand the compressed raw clusters into an array of 1024 channels and redo the clusterization using a more sophisticated offline algorithm. The basis of the algorithm is to find a cluster seed which is defined as a local signal maximum with a signal-to-noise ratio, $S/N > 4.0$, and to form the cluster by collecting all the strips with $S/N > 1.0$ neighboring the seed. Special cases such as a multi peak or near border clusters are treated by taking into account the actual geometry of the tracker. The cluster coordinate in units of readout channels is calculated as the Center-of-Gravity (CoG) of the collected cluster elements weighted by the ADC signals.

The geometrical coordinate within the ladder is obtained from the readout channel according to the nominal strip positions in the design. For the n-side, the routing scheme of the cable distributes the strip signals of alternating sensors to the same readout channel, i.e. the first (second) 192 of the 384 readout channels correspond to the strips of sensors $1,3,5,\ldots$ $(2,4,6,\ldots)$. A different bonding scheme of the ladders placed on the external planes is also taken in account.

The second step of the reconstruction process is to combine the coordinates defined by clusters on the p- and n-sides into a three dimensional hit. As shown in Fig. 2, the AMS master reference system is defined with an x-axis along the main component of the magnetic field, a z-axis normal to the tracker planes pointing upward, and a y-axis to complete a right handed system. The ladders are placed parallel to the x-axis and the coordinate in the p (n)-side corresponds to the y (x)-coordinate in the AMS master reference system. In the present algorithm any possible combination generates a hit and the ambiguity is resolved later by the track finding algorithm. The coordinates of the three dimensional hit ($\boldsymbol{V}_G$) are obtained from its position within the ladder ($\boldsymbol{V}_L$) with the nominal position ($\boldsymbol{V}_L$) and orientation (R_L) of the ladder within the AMS master reference as: $\boldsymbol{V}_G = R_L\boldsymbol{V}_L + \boldsymbol{V}_L$. $\boldsymbol{V}_L$ and R_L have been calculated from the design data and a measurement during the integration and stored in a tracker offline database.

The mechanical positioning precision of the tracker assembly of about 100 μm is much worse than the track position measurement which has the intrinsic resolution of $\sim 10(30)\,\mu$m in the y (x)-coordinate. An accurate knowledge of the ladder geometry with a precision of a few μ m is required to maximize the tracker performance. Ladder alignment parameters, $\boldsymbol{V}_A$ and R_A, are introduced to correct for a displacement and a rotation, respectively, so that the aligned hit position is obtained as: $\boldsymbol{V}_G = (R_L R_A)\boldsymbol{V}_L + (\boldsymbol{V}_L + \boldsymbol{V}_A)$. The alignment parameters have been evaluated using the procedure discussed in Section 4.3.

4.2. Track finding and fitting

In order to reconstruct a particle track, a set of hits associated with the track has to be distinguished from the noise hits, hits associated with the other tracks as well as ghosts generated by the routing scheme.

In this analysis a simple track finding algorithm has been applied. The hit list is scanned and tested for the consistency with a single straight line fit. Combinations with a too large χ^2 are rejected. The algorithm accepts up to three layers out of eight with no hit along the track due to the inactive region of about 7% in each sensor. Track candidates are accepted in the order of: (1) the larger number of associated hits and (2) the smaller fitting χ^2. The associated hits of the accepted tracks are marked and not used for the other tracks. The track finding process is iterated until no more track is found or the number of tracks reaches a maximum of two.

4.3. Ladder alignment

The fitting residuals of each ladder include the intrinsic resolution of the sensors, the multiple scattering error, and the mechanical precision of the assembly. The first two make the residual width wider and the third one shifts the residual mean. The alignment parameters can be therefore estimated from the distribution of the residuals.

In the ideal case, where the track position is exactly known and the ladder under analysis has the perfect resolution, the elements of the alignment parameters, $\boldsymbol{V}_A$ and R_A are obtained by the following formulae:

$$V_{Ax} = \rho_x \tag{1}$$

$$V_{Ay} = \rho_y \tag{2}$$

$$V_{Az} = \rho_x/p_{xz} = \rho_y/p_{yz} \tag{3}$$

$$\tan\alpha = \rho_y/(h_x - h_{x0}) = \rho_x/(h_y - h_{y0}) \tag{4}$$

$$\tan\beta = \rho_x/[p_{xz}(h_x - h_{x0})] = \rho_y/[p_{yz}(h_x - h_{x0})] \tag{5}$$

$$\tan\gamma = \rho_x/[p_{xz}(h_y - h_{y0})] = \rho_y/[p_{yz}/(h_y - h_{y0})] \tag{6}$$

where α, β, and γ are rotation angles of R_A defined as follows:

$$R_A = R_\alpha R_\beta R_\gamma \tag{7}$$

$$R_\alpha = \begin{pmatrix} \cos\alpha & \sin\alpha & 0 \\ -\sin\alpha & \cos\alpha & 0 \\ 0 & 0 & 1 \end{pmatrix} \tag{8}$$

$$R_\beta = \begin{pmatrix} \cos\beta & 0 & -\sin\beta \\ 0 & 1 & 0 \\ \sin\beta & 0 & \cos\beta \end{pmatrix} \tag{9}$$

$$R_\gamma = \begin{pmatrix} 1 & 0 & 0 \\ 0 & \cos\gamma & \sin\gamma \\ 0 & -\sin\gamma & \cos\gamma \end{pmatrix}. \tag{10}$$

ρ_x and ρ_y are the mean residuals, p_{xz} and p_{yz} are projected track inclinations ($\Delta x/\Delta z$ and $\Delta y/\Delta z$), h_x and h_y are the hit positions, and h_{x0} and h_{y0} are the position of the geometric center.

The ladder has a finite resolution, and the predicted track position has uncertainties from the resolution and mechanical precision of the other ladders as well as from multiple scattering. Thus the alignment parameters are estimated by taking ρ_x and ρ_y as the Gaussian mean of the residual distribution. The event sample is selected to have only one track and with a loose cut on the χ^2 of the fitting to avoid large scattering events. The estimation of the alignment parameters is iteratively made so as to improve the predicted track position by applying the alignment parameters estimated in the previous iteration. To minimize the coupling between different coordinates the parameters have been estimated in the following order:

(1) Estimation of values for V_{Ax} and V_{Ay} from nearly vertical tracks.
(2) Estimation of values for V_{Az} from inclined tracks.
(3) Estimation of V_{Ax}, V_{Ay}, V_{Az}, and tanα.
(4-15) Estimation of V_{Ax}, V_{Ay}, V_{Az}, tanα, and tanβ.

The ladder inclination along the ladder length, tanγ, has not been estimated and assumed as tan$\gamma = 0$ because the lever arm is small (~ 3.5 cm).

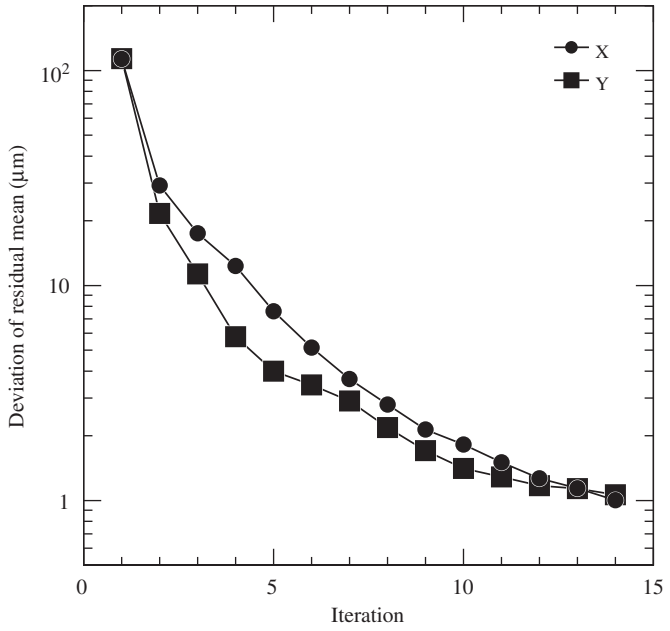

Fig. 6. Development of the deviation of the residual mean at each iteration of the alignment correction. The deviation is defined as the RMS of the residual mean distribution for 190 tracker ladders.

5. Performance

In this section, results of cosmic-ray data analysis are presented and discussed focusing on the tracker alignment and position resolution.

5.1. Alignment calibration and its stability

According to the procedure given in Section 4.3, five alignment correction parameters were estimated for each ladder using the M000 data set as given in Table 1. As a figure of merit, we use the RMS width of the distribution of the mean residuals for all ladders. Fig. 6 shows the development of this width as a function of the alignment iterations. Convergence to the level of 1 μm is observed after < 15 iterations. Distributions of the obtained five alignment parameters for all ladders are shown in Fig. 7. The distributions are centered around zero and have a width of about 100 μm as expected from the mechanical precision

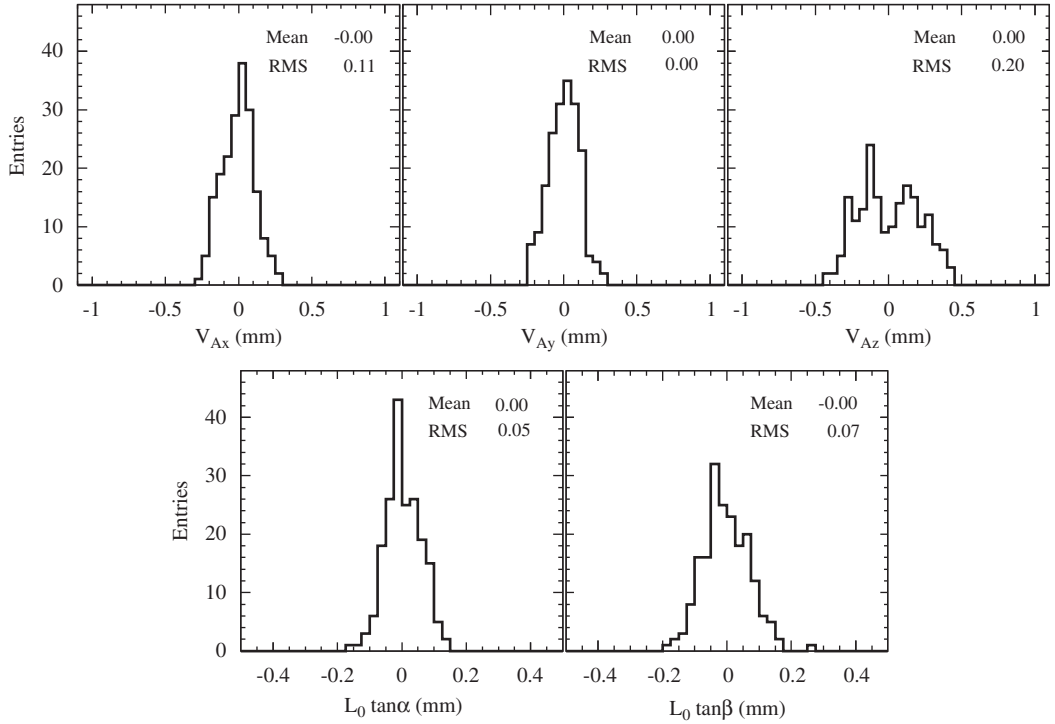

Fig. 7. Distributions of five alignment parameters for all the ladders obtained from the data set M000. The rotation angles (α and β) are given as tanα and tanβ multiplied by a mean half ladder length, $L_0 = 24.4$ cm. Mean and root mean square (RMS) values are also shown.

of the assembly. The reduced accuracy in the z-coordinate is tolerable since this represents the coordinate along the tracker direction.

In order to have a 10 μm position resolution, an alignment accuracy of a few μm is required. In absence of an external position reference. the reproducibility of the obtained results with different data samples has been used to evaluate the robustness of the alignment method and the stability of its results. Different alignment parameter sets ($P_{M001}-P_{M005}$) were evaluated in five independent sub-samples of the available statistics, M001–M005, as given in Table 1. The differences between the $P_{M001}-P_{M005}$ parameter sets and those obtained with the full data sample (P_{M000}) were analyzed. The Gaussian widths of the difference distributions are given in Table 2 for the five sub-samples; no significant shifts were found in the mean values of the distributions.

To check the dependence of the alignment results on the statistics used to determine the parameters, the same study was performed with reduced data samples, using only a fraction of the available statistics. Fig. 8 shows the statistical dependence of the alignment accuracy estimated with the Gaussian width of the differences between the V_{Ax}, V_{Ay}, V_{Az} parameters evaluated in the reduced samples and in the reference set. In each panel, the Gaussian width, σ, as a function of the number of tracks used in the alignment, N, is shown. The distributions are well described by the functional form, $\sigma = p_0 + p_1/\sqrt{10^{-6}N}$.

In the alignment procedure, ladders are considered as rigid units composed of silicon sensors regularly spaced with centers aligned along the ladder length. A possible displacement of the sensors from their nominal positions in each ladder was checked after the alignment corrections. Alignment parameters for the displacement in the x- and y- coordinate, V_{Ax} and V_{Ay} have been estimated for each sensor applying the same procedure used in the ladder alignment. In this case V_{Ax} and V_{Ay} were obtained as relative values with respect to the aligned ladder position, so that the local displacements can be estimated. Gaussian width of the distribution of the sensor displacement was obtained as 4.0 and 4.2 μm in the x- and y-coordinates, respectively. These values are comparable with the corresponding metrology measurements performed after ladder assembly, 4.6 and 3.9 μm [5].

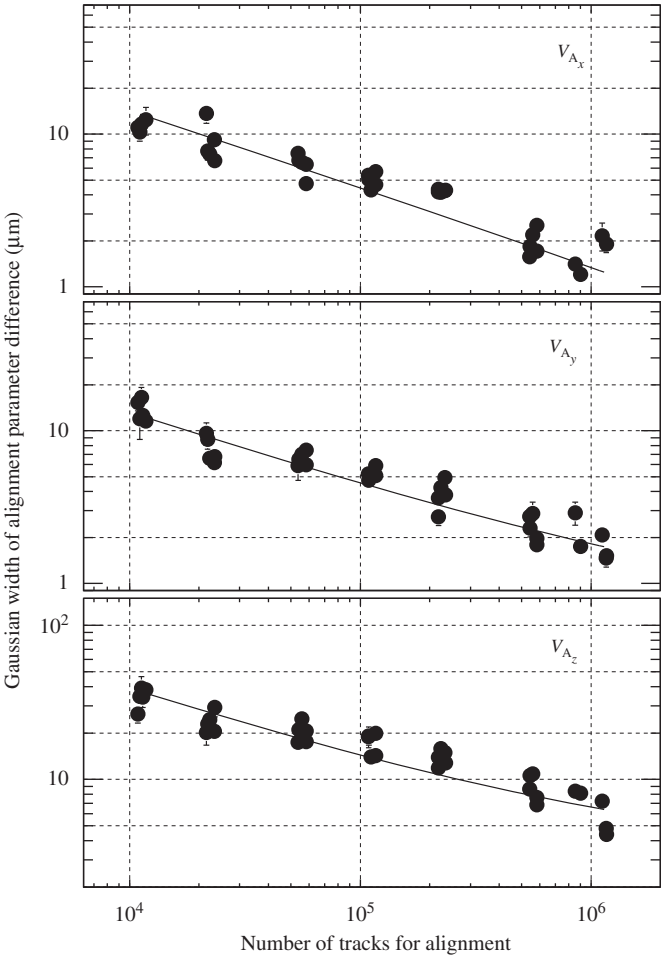

Fig. 8. Statistical dependence of the alignment accuracy estimated as a Gaussian width of difference between a statistically reduced sample and the reference parameter for parameters, (from top panel to bottom) V_{Ax}, V_{Ay}, and V_{Az}. For each panel the Gaussian width, σ was fitted with a function of number of tracks for the alignment, N as $\sigma = p_0 + p_1/\sqrt{10^{-6}N}$ with $p_0 = -0.09 \pm 0.08$ and $p_1 = 1.43 \pm 0.04$ for V_{Ax}, $p_0 = 0.56 \pm 0.09$ and $p_1 = 1.26 \pm 0.05$ for V_{Ay}, and $p_0 = 3.00 \pm 0.27$ and $p_1 = 3.61 \pm 0.13$ for V_{Az}.

5.2. Mechanical stability

During the period from 10 to 14 June 2008, the mechanical stability of the tracker structure was checked by rotating the AMS spectrometer around the y-axis at different angles up to $\pm 90^\circ$ as given in Table 1. The level of mechanical distortions possibly induced by gravity was evaluated by the analysis of the data sets recorded at each step of the rotation. For each step we evaluated the alignment parameters and compared them with the reference ones obtained with the data taken prior to the rotation in the same way as described in Section 5.1. No significant shift in the alignment parameters was found within the statistical accuracy as estimated from Fig. 8. It should be noted that the Gaussian widths of the alignment parameter difference between the data sets, M000 and J001 (before and after the rotation), were 1.7 ± 0.2, 1.9 ± 0.2, and 6.7 ± 0.6 μm for V_{Ax}, V_{Ay}, and V_{Az}, respectively. We conclude that the tracker structure is rigid and stable against the rotation at a level of 10^{-6} (less than a few μm out of 1 m).

Table 2
Gaussian width of the distribution of difference in alignment parameters between each data set and the reference data set (M000).

Data set	V_{Ax} (μm)	V_{Ay} (μm)	V_{Az} (μm)	$L_0\tan\alpha$ (μm)	$L_0\tan\beta$ (μm)
M001	2.1 ± 0.1	2.9 ± 0.2	11.6 ± 0.9	3.2 ± 0.3	10.3 ± 1.1
M002	2.3 ± 0.2	2.3 ± 0.2	9.8 ± 0.7	2.9 ± 0.3	9.2 ± 0.8
M003	1.5 ± 0.1	1.7 ± 0.1	7.6 ± 0.8	2.2 ± 0.2	9.7 ± 0.7
M004	2.2 ± 0.2	1.7 ± 0.2	8.4 ± 0.8	2.4 ± 0.2	10.7 ± 0.8
M005	1.7 ± 0.1	2.5 ± 0.4	10.5 ± 0.9	1.8 ± 0.1	11.9 ± 1.0
Average	2.0 ± 0.1	2.2 ± 0.1	9.6 ± 0.4	2.5 ± 0.1	10.4 ± 0.4

Gaussian width for the rotation angles (α and β) are given as $\tan\alpha$ and $\tan\beta$ multiplied by a mean half ladder length, $L_0 = 24.4$ cm to show the effect on the position resolution clearly.

5.3. Position resolution

The width of the residual distribution after the alignment calibration has been used to estimate the average position resolution of the tracker ladders at different particle incident angles. To minimize the uncertainty in the impact point prediction only tracks which have associated hits in all eight layers have been considered, and the tracks are re-fitted with seven hit points except the one under study. A tight cut on the χ^2 of the track fitting has been applied to reject low momentum tracks poorly

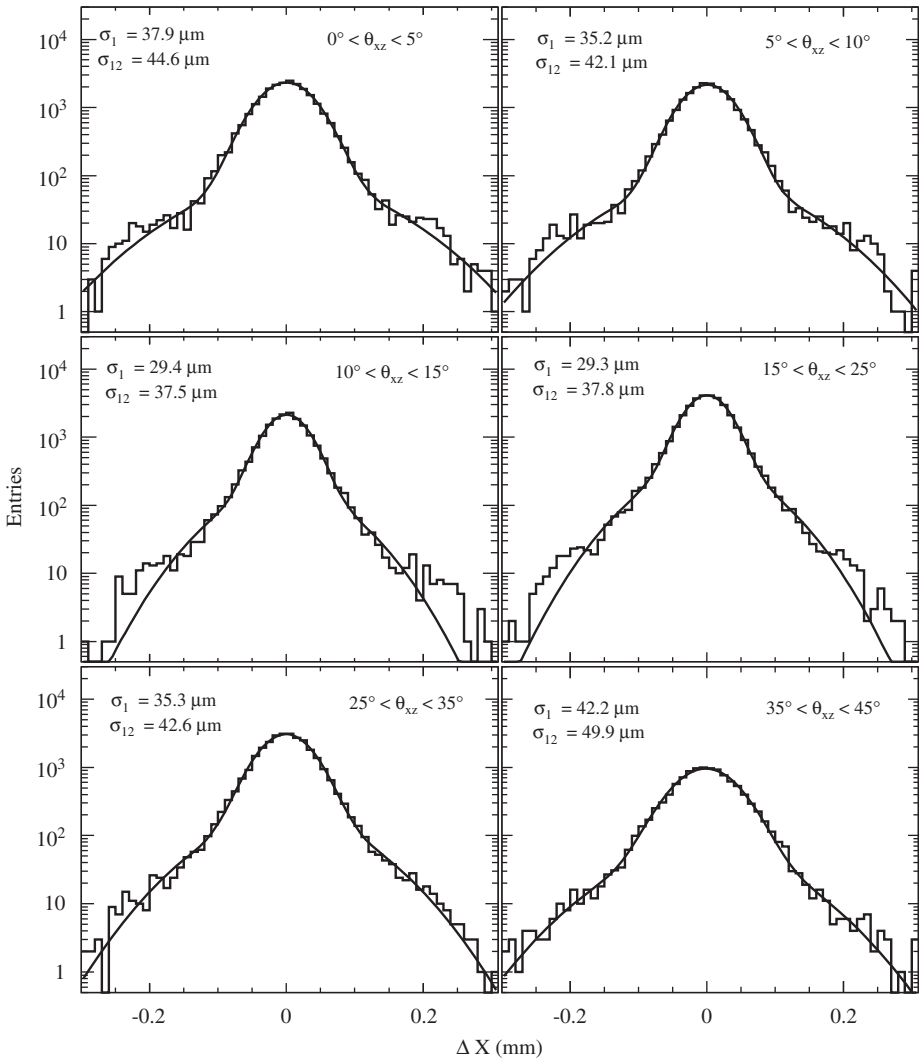

Fig. 9. The residual distributions in x-coordinate (seven point fit to eight layers) for each angle bin. The residual distributions are described with a sum of two Gaussians; the narrower Gaussian width (σ_1) and the area-weighted average width of the two Gaussians are indicated (σ_{12}).

reconstructed due to multiple scattering in the detector material. Fig. 9 and Fig. 10 show residual distributions in the x- and y- coordinate, respectively, obtained for six angle intervals, $0^\circ < \theta < 5^\circ$, $5^\circ < \theta < 10^\circ$, $10^\circ < \theta < 15^\circ$, $15^\circ < \theta < 25^\circ$, $25^\circ < \theta < 35^\circ$, and $35^\circ < \theta < 45^\circ$, where θ is a projected angle onto a plane with the z-axis and the axis under analysis. The residual distributions are described with a sum of two Gaussians; the narrower Gaussian width (σ_1) and the area-weighted average width of the two Gaussians are indicated (σ_{12}). The multiple-Gaussian shape of the residual distributions can be understood by the fact that the position resolution depends on the relative position of the particle in the gap between two consecutive readout strips as discussed in detail in Ref. [2].

With the assumption that the resolutions of all the ladders are the same, the average ladder resolution was obtained by comparing the observed residual distributions with those estimated by a GEANT3 [7] simulation following the same approach as Ref. [2]. In the simulation, track coordinates were randomized around their true values according to a single Gaussian distribution corresponding to a given nominal resolution. Different simulation runs were made varying the nominal resolutions between 10 and 30 μm for the y-coordinate measurement and between 20 and 50 μm for the x-coordinate measurement. In the present case, the projected track position has a significant uncertainty arising from the multiple scattering effect, which has been simulated by modeling the momentum spectrum of the incident cosmic muons estimated for the CERN location (46.2°N, 6.1°E, 430 m ASL) [6]. In the bottom panel of Fig. 11 the muon momentum distribution used in the simulation is presented together with the distributions after the χ^2 cuts in x- and y-coordinates in this analysis, respectively. The dependence of the χ^2 on the incident momentum is also shown.

The linear dependence of the residual widths on the position resolution assumed in the simulation is presented in Fig. 12: due to multiple scattering and geometrical effects, different behaviors characterize the inner and outer tracker layers. Data points corresponding to σ_{12} at different incident angles are also shown. The average position resolution is estimated from a comparison between the residual widths observed in the data and their expected dependence on resolution as evaluated with the simulation. The estimated position resolution in the x (y)- coordinate is shown in Fig. 13 as a function of the projected angle, θ_{xz} (θ_{yz}). Results are presented in two manners as in Ref. [2]: the effective resolution obtained from the area-weighted average width of the two Gaussians (σ_{12}), and the optimal resolution

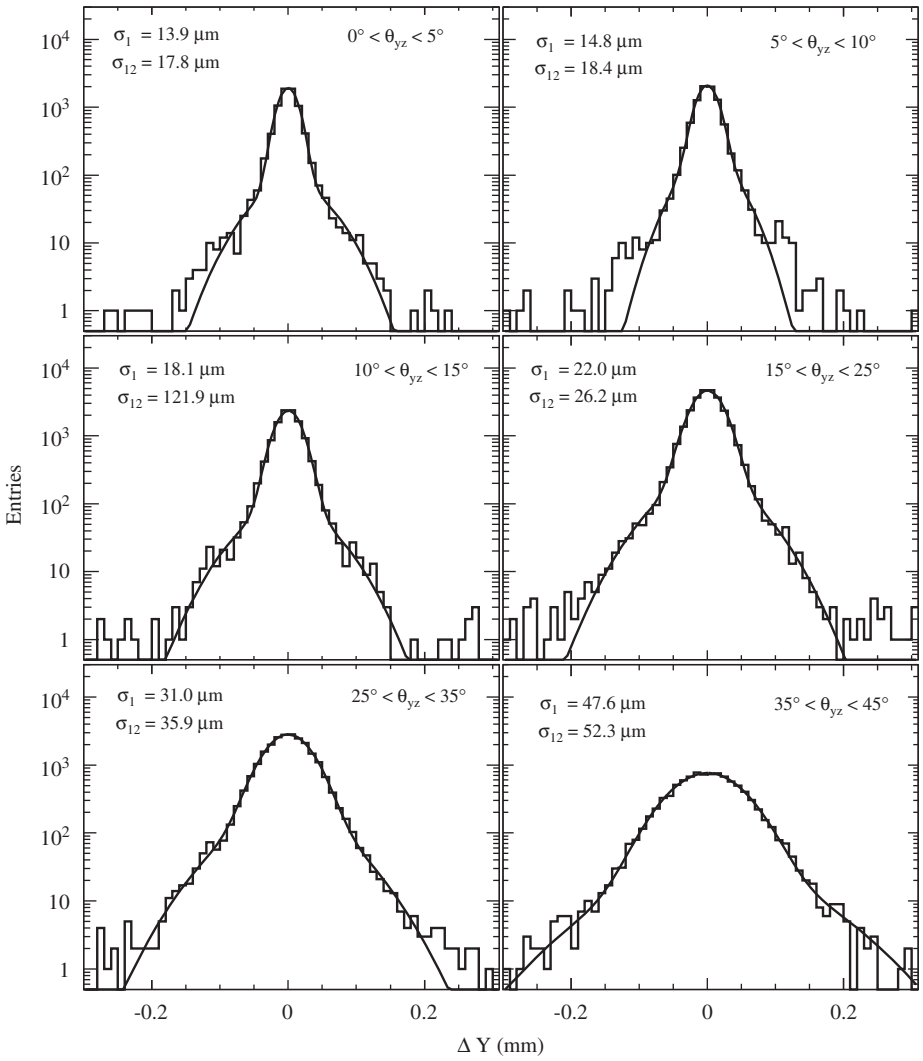

Fig. 10. The residual distributions in *y*-coordinate (seven point fit to eight layers) for each angle bin. The residual distributions are described with a sum of two Gaussians; the narrower Gaussian width (σ_1) and the area-weighted average width of the two Gaussians are indicated (σ_{12}).

obtained from the narrower Gaussian width (σ_1). Due to the larger strip pitch on the ohmic side, the resolution in the *x*-coordinate worsens slightly at the vertical incidence, since charge is shared among fewer strips. The optimal resolution in the *y*-coordinate at the vertical incidence is consistent with a result obtained in a proton test beam in 2002 [2] as shown in the same figure. It should be noted that two data points of test beam results at 15° and 30° are obtained only by a single inclined ladder and the setup was not fully optimized.

The dependence of the position resolution on the statistics used to calibrate the alignment parameters has also been studied following the same approach as used to evaluate the robustness of the alignment method (Section 5.1). Fig. 14 shows the optimal position resolution, σ as a function of the number of tracks used for the alignment, *N*, for three intervals of the projected angles, (a) $0^\circ < \theta < 5^\circ$, (b) $10^\circ < \theta < 15^\circ$, and (c) $25^\circ < \theta < 35^\circ$. Results are presented for both *x*- and *y*- coordinates in three incident angle intervals. Data points were described by the function $\sigma = p_0 + p_1/\sqrt{10^{-5}N}$, confirming the statistical dependence of the alignment accuracy discussed in Section 5.1. Taking into account the measured event rate of 37 Hz as expected for the cosmic muons on the ground and an expected event rate of ~ 100 Hz for AMS-02 on the ISS[5], we conclude that one day of data taking prior to charging the AMS-02 superconducting magnet should be enough to calibrate the tracker alignment with more than 10^6 straight tracks.

We have also studied a relation between the position resolution and the cluster signal-to-noise ratio for each ladder instead of averaging all the ladders. The cut on the χ^2 of the track fitting was loosened to have enough statistics. The resolution has been estimated from the difference of the position measurement between layers mounted on two sides of the same plane, since the two layers are separated each other only by 4 cm and the effect of multiple scattering has been kept minimum even under the loose χ^2 cut. Fig. 15 shows the estimated position resolution in the *x*- and *y*-coordinate as a function of signal-to-noise ratio for vertical ($\theta < 5^\circ$) incidence. Results obtained in a proton test beam in 2003 [2] are also shown in the same figure. The data points of the test beam are fitted by linear functions and extrapolated to higher signal-to-noise ratio. The results in this analysis are consistent with those in the test beam.

[5] For a 12 GV cut off rigidity around the equator.

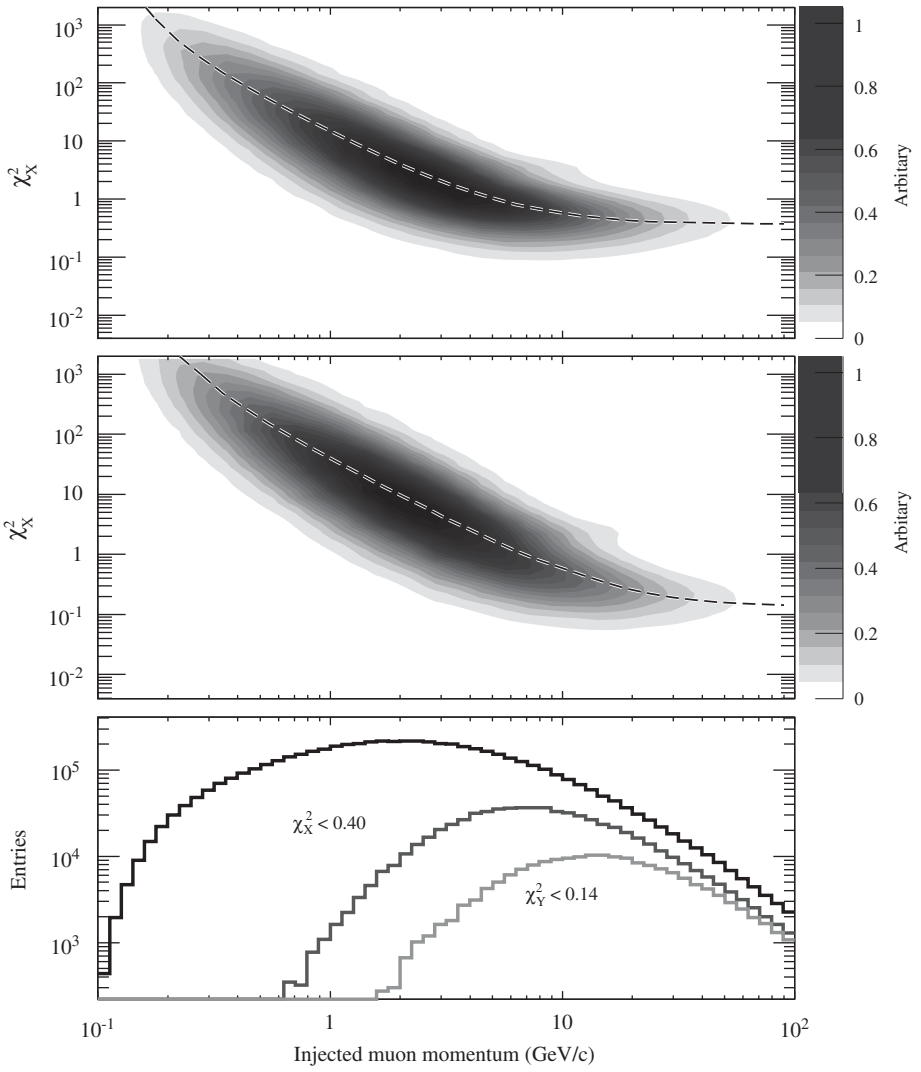

Fig. 11. χ^2 distribution as a function of injected momentum for x (top) and y (middle) coordinates estimated by the Geant3 simulation for vertical ($\theta < 5^\circ$) incidence. The dashed lines show the peak position of the χ^2 distribution. The momentum distribution of the incident cosmic muons estimated for the CERN location is also shown in the bottom panel together with the distribution after the χ^2 cuts, $\chi^2_x < 0.40$ and $\chi^2_y < 0.14$.

5.4. Expected rigidity resolution

We have estimated the expected rigidity resolution with a Geant3 [7] simulation, where the hit positions are randomized by a single Gaussian with its width defined as a function of the projected track inclination angle according to the effective position resolution estimated from the cosmic-ray data. The top panel of Fig. 16 shows the position resolution in the y-coordinate (the bending direction) assumed in the simulation together with the data points obtained from the cosmic-ray data. The rigidity resolution was estimated for tracks with measurements in at least six tracker layers including the two external ones. The distribution of measurements of the magnetic deflection, η ($\eta \equiv 1/R$, inverse of the rigidity) is approximately Gaussian, and its width, σ_η is independent of the incident rigidity in the high energy region where multiple scattering is negligible. The performance of a magnetic spectrometer is then characterized by the maximum detectable rigidity (MDR) corresponding to a measurement error of 100% and obtained as $1/\sigma_\eta$. The middle panel of Fig. 16 shows the estimated MDR as a function of the inclination angle for 1 TV proton incidence. The angle distribution in the geometric acceptance of the tracker is also shown in the bottom panel of the same figure. In spite of the large dependence of the position resolution on the incident angle (a factor of 2.8 between 0° and 40°), a much reduced variation is found for the MDR (27%). This can be understood that the deflection resolution, σ_η has a dependence on the effective track length, $L = L_0/\cos\theta_{yz}$, and the position resolution in the coordinate perpendicular to the track, $\sigma_\perp = \sigma_y \cos\theta_{yz}$, as

$$\sigma_\eta \propto \sigma_\perp/L^2 = \sigma_y \cos^3\theta_{yz}/L_0^2$$

where L_0 and σ_y are the distance between external planes and the position resolution in the y-coordinate, respectively. The factor, $\cos^3 40^\circ \simeq 0.45 \simeq 1.27/2.8$ is consistent with the difference in the factors between the position resolution (2.8) and the MDR (1.27).

Fig. 17 shows the rigidity resolution as a function of the injected rigidity estimated by the same simulation for the proton incidence in the whole tracker acceptance. In the region above 100 GV, the rigidity resolution is determined by the tracker resolution with the estimated MDR of 2.3 TV, while in the low rigidity region below 50 GV, it is determined by multiple scattering as $\Delta R/R \sim 2\%$. Another possible source affecting the rigidity measurement is the uncertainty of the magnetic field

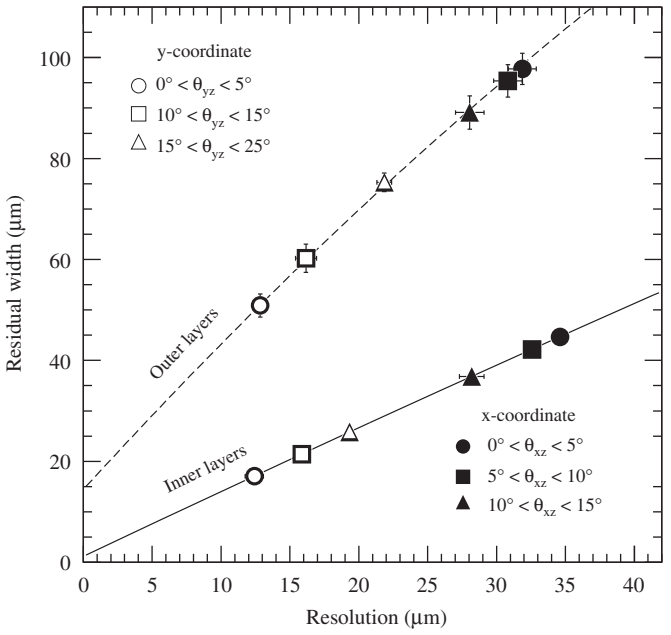

Fig. 12. The relation between residual width and position resolution obtained by a simulation. The solid and dashed lines show the relations for the inner and outer layers, respectively. Open and closed markers show data points obtained as the area-weighted average width (σ_{12}) of the two Gaussians of the residual distributions in the *x*- and *y*-coordinates, respectively, for each angle bin as indicated in the figure.

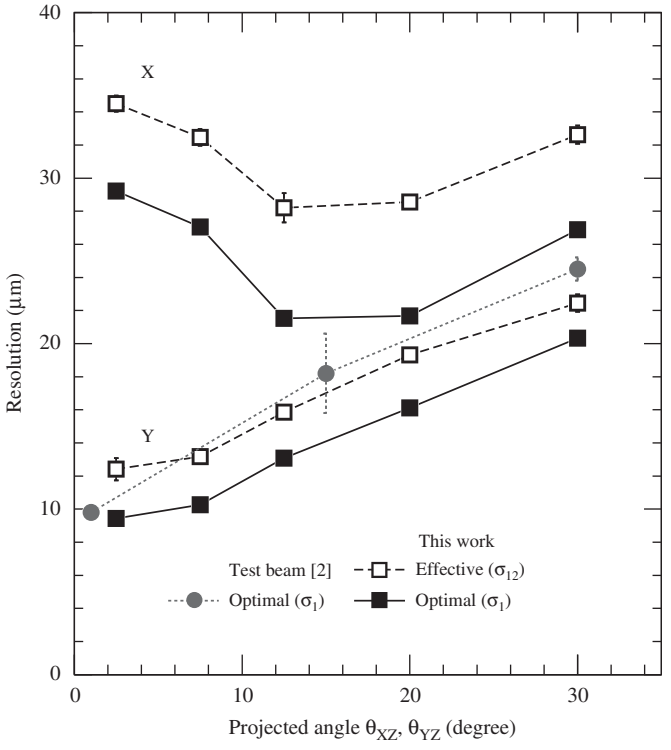

Fig. 13. The position resolution in the *x*- (upper points) and *y*- (lower points) coordinates estimated as a function of the projected angle, θ_{xz} and θ_{yz}. Results of two different Gaussian width, σ_{12} and σ_1 are shown, where σ_{12} and σ_1 indicate the effective and optimal performance, respectively. Proton test beam results [2] are also shown. It should be noted that two data points of test beam results at 15° and 30° are obtained only by a single inclined ladder and the setup was not fully optimized.

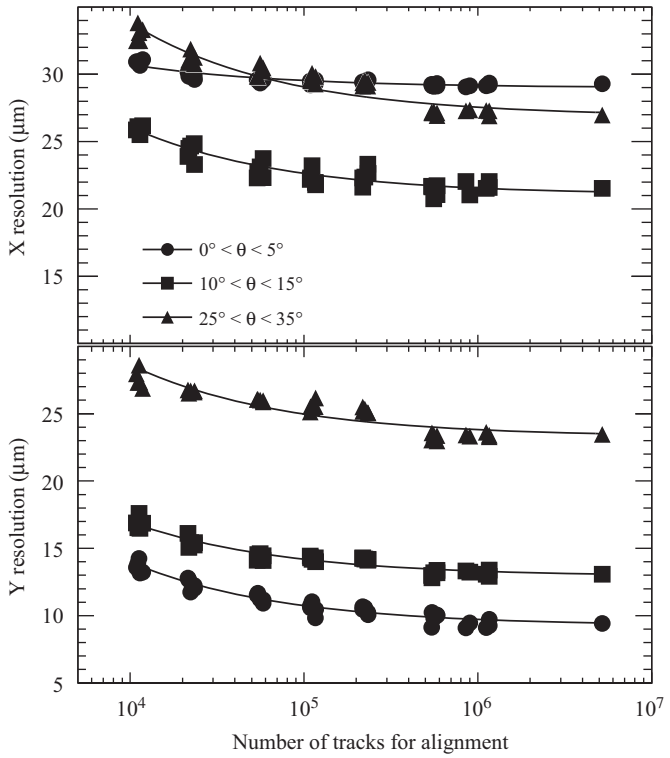

Fig. 14. The position resolution estimated from the narrower Gaussian width in the *x*- (top) and *y*- (bottom) coordinates as a function of number of tracks used for the alignment for three angle bins, (1) $0^\circ < \theta < 5^\circ$ (closed circles), (2) $10^\circ < \theta < 15^\circ$ (closed squares), and (3) $25^\circ < \theta < 35^\circ$ (closed triangles). Data points in the *x*-coordinate were described by a function $\sigma = p_0 + p_1/\sqrt{10^{-5}N}$ with $p_0 = 9.25 \pm 0.05$ and $p_1 = 1.50 \pm 0.03$ for (1), $p_0 = 12.91 \pm 0.05$ and $p_1 = 1.28 \pm 0.03$ for (2), and $p_0 = 23.28 \pm 0.07$ and $p_1 = 1.69 \pm 0.06$ for (3). Data points in the *y*-coordinate were described by the same function with $p_0 = 28.99 \pm 0.06$ and $p_1 = 0.54 \pm 0.04$ for (1), $p_0 = 21.04 \pm 0.11$ and $p_1 = 1.59 \pm 0.07$ for (2), and $p_0 = 26.85 \pm 0.07$ and $p_1 = 2.20 \pm 0.05$ for (3).

which mainly arises from the displacement of the tracker with respect to the magnet coordinate. We expect the accuracy and the stability of the support structure between the tracker and the magnet to be < 1 mm. We have studied the effect on the rigidity resolution caused by the displacement of the magnet by artificially shifting its coordinate with respective to the tracker. Fig. 17 also shows the rigidity resolutions in the cases that the coordinate of the magnetic field is shifted by 5 mm along *x*-, *y*-, and *z*-axis, where multiple scattering is switched off in the simulation to clearly see the effect of the shifts. As seen in the figure the effect is negligible compared with that of multiple scattering.

6. Conclusion

During the pre-integration phase of the AMS-02 spectrometer for 10 months, we have accumulated 90 million events of cosmic-ray muon data for the tracker under a stable condition. The positions of all elements agree with their design ones with the required accuracy of 100 μm. Using the data of nominal condition runs, We have estimated the stability in the calibration of alignment parameters as 1.5 ± 0.1, 2.2 ± 0.1, and 7.1 ± 0.3 μm for the translations along three axes, V_{Ax}, V_{Ay}, and V_{Az}, respectively. We have also estimated the position resolution for nearly vertical incidence ($\theta < 5^\circ$) as 9.6 μm (29.2 μm) in the *y* (*x*)-coordinate as an optimal resolution, and 12.6 μm (34.7 μm) in

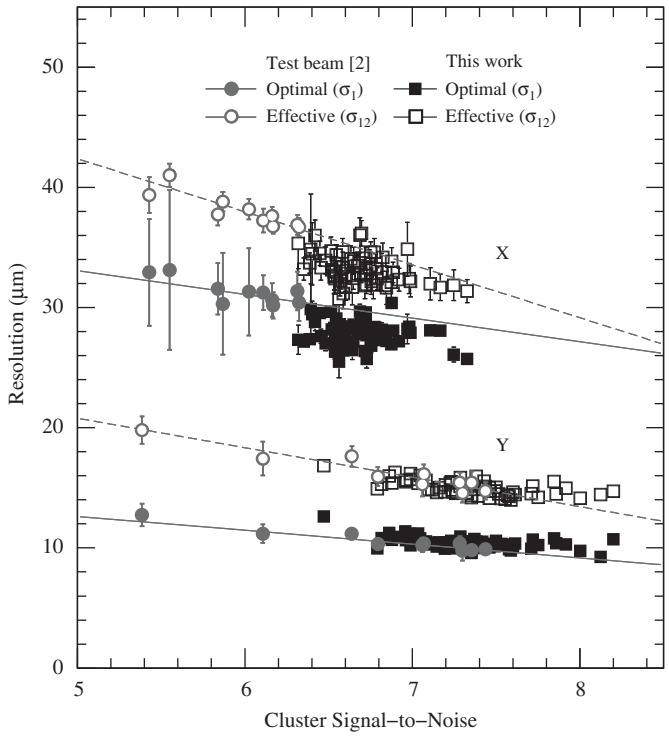

Fig. 15. The position resolution in the *x*- (upper points) and *y*- (lower points) coordinates estimated as a function of the cluster signal-to-noise ratio for vertical ($\theta < 5^{\circ}$) incidence. Results of two different Gaussian width, σ_{12} and σ_1 are shown, where σ_{12} and σ_1 indicate the effective and optimal performance, respectively. Proton test beam results [2] are also shown. The lines are obtained by fitting data points of the test beam and extrapolated to the higher signal-to-noise range.

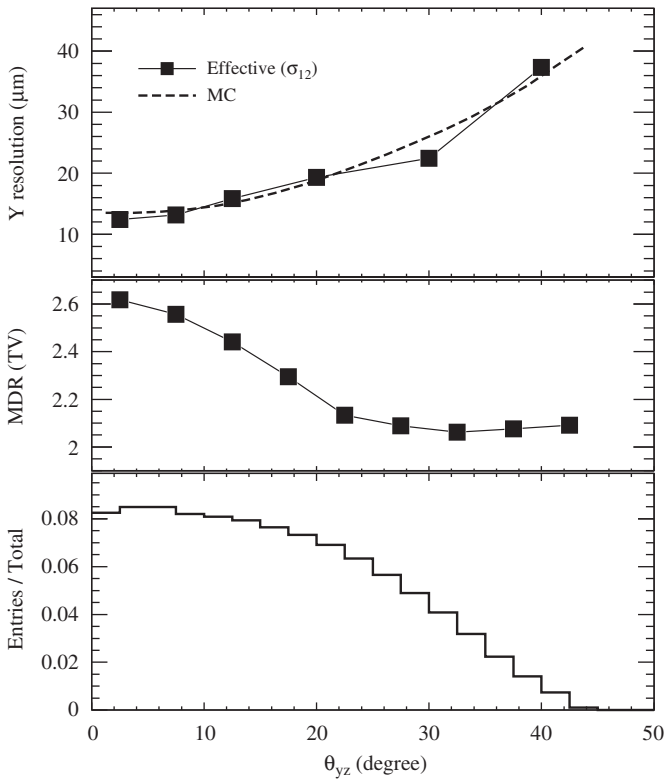

Fig. 16. The effective position resolution (weighted average of two Gaussian widths) in the *y*-coordinate for different inclination angles (top), the Maximum Detectable Rigidity (MDR, 100% rigidity measurement error) as a function of the inclination angle estimated for 1 TV proton incidence with the simulation (middle), and the inclination angle distribution in the geometric acceptance of the tracker (bottom).

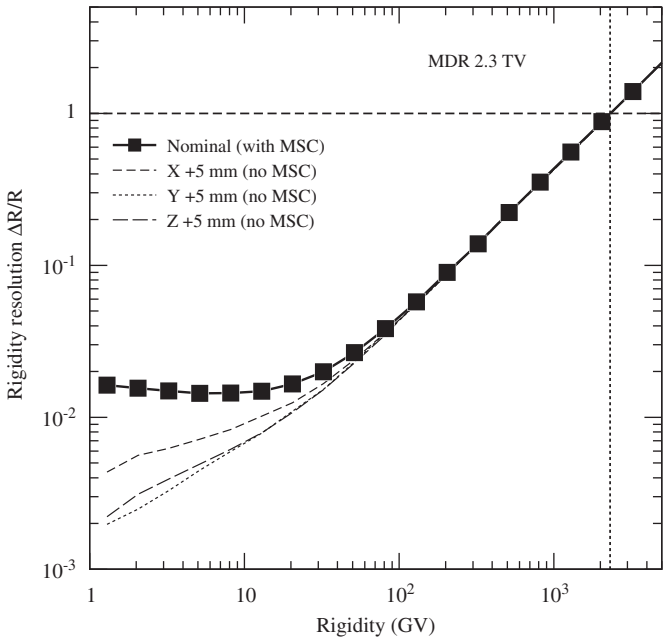

Fig. 17. Relative rigidity resolution as a function of the injected rigidity for protons in the whole tracker acceptance estimated in the simulation (solid squares) with the maximum detectable rigidity indicated. Rigidity resolutions in the cases that the coordinate of the magnetic field is shifted by 5 mm along *x*- (dashed curve), *y*- (dotted curve), and *z*-axis (dash-dotted curve) are also shown, where multiple scattering (MSC) is switched off in the simulation to clearly see the effect of the shifts.

the *y* (*x*)- coordinate as an effective resolution, and their dependence on the incident angle. The dependence of the position resolution on the statistics of tracks for the alignment calibration indicates that a corresponding sample can be accumulated under flight conditions within a day. The estimated position resolution was implemented into the simulation as a function of incident angle and the average rigidity resolution corresponds to a maximum detectable rigidity of 2.3 TV for protons averaged over the full acceptance.

Acknowledgments

We wish to thank our colleagues in AMS-02 and in particular: X. Cai, M. Capell, A. Kounine, V. Koutsenko, A. Lebedev, and M. Vergain of the Massachusetts Institute of Technology; S. Bizzaglia of INFN Perugia; Ph. Bouvier, M. Weber, and M. Willenbrock of l'Université de Genève; B. Verlaat of NIKHEF; and C. Gargiulo of INFN Roma. This work was partly funded by the Agenzia Spaziale Italiana (ASI Contract 035/07, AMS-02–Fase E2 ed analisi dati). This work was funded in part by the Swiss National Fund for Science Research.

References

[1] M. Aguilar, et al., Phys. Rep. 366 (2002) 331.
[2] J. Alcaraz, et al., Nucl. Instr. and Meth. A 593 (2008) 376.
[3] B. Alpat, et al., Nucl. Instr. and Meth. A 540 (2005) 121.
[4] M. Pauluzzi, Nucl. Instr. and Meth. A 473 (2001) 67.
[5] W.J. Burger, Nucl. Instr. and Meth. A 582 (2007) 886.
[6] T. Sanuki, et al., Phys. Rev. D 75 (2007) 043005;
M. Honda, et al., Phys. Rev. D 75 (2007) 043006 and M. Honda, private communication (2008).
[7] R. Brun, et al., CERN Report DD/EE/84-1, revised 1987.